PCCP

Accepted Manuscript

ROYAL SOCIETY OF CHEMISTRY

www.rsc.org/pccp

Physical Chemistry Chemical Physics
CREATED USING THE RSC LaTeX PCCP ARTICLE TEMPLATE – SEE www.rsc.org/electronicfiles FOR DETAILS
ARTICLE TYPE www. rsc.org/xxxxxx | XXXXXXXX

Local order and long range correlations in imidazolium halide ionic liquids: a combined molecular dynamics and XAS study

Valentina Migliorati,*[a], Alessandra Serva[a], Giuliana Aquilanti,[b] Sakura Pascarelli,[c] and Paola D'Angelo*[a]

Received Xth XXXXXXXXXX 20XX, Accepted Xth XXXXXXXXX 20XX
First published on the web Xth XXXXXXXXXX 200X
DOI: 10.1039/b000000x

A thorough characterization of the structural properties of alkylimidazolium halides ionic liquids (ILs), namely 1-alkyl-3-methylimidazolium bromide ([$C_n$mim]Br with n = 5, 6, 8, 10) and iodide ([C_6mim]I), has been carried out by combining Molecular Dynamics simulations and the EXAFS spectroscopy. The existence of a local order in [$C_n$mim]Br ILs has been evidenced, with anions and imidazolium head groups forming a local three-dimensional bonding pattern that is common to all the [$C_n$mim]Br IL family, regardless the length of the alkyl chain attached to the cation. On the other hand, upon alkyl chain elongation significant differences have been highlighted in the long-range structure of these ILs. Theoretical X-ray structure factors have been calculated starting from the MD simulations and a low q peak has been found for all [$C_n$mim]Br ILs, indicating the existence of long-range structural correlations. The low q peak moves to smaller q values corresponding to longer distances, increases in intensity and sharpens with increasing alkyl chain length on the cation. Similarities and differences between the ion three-dimensional arrangements in [C_6mim]Br and [C_6mim]I were highlighted and the structural arrangement of Br^- and I^- was found to be different in the proximity of the most acidic hydrogen atom of the imidazolium ring: the I^- ion is preferentially located above and below the ring plane, while the Br^- ion has a high probability also to be coplanar with the imidazolium ring. A quantitative analysis of the Br and I K-edge EXAFS spectra of alkylimidazolium halides ILs has been carried out starting from the microscopic description of the systems derived from MD simulations. A very good agreement between theoretical and experimental EXAFS signals has been obtained, allowing us to assess the reliability of the MD structural result for all the alkylimidazolium halides ILs investigated in this work.

1 Introduction

Research on Ionic Liquids (ILs) has been witnessing an extraordinary growth during the last years and the fascinating properties of this new class of materials have inspired a huge variety of applications. The appeal of ILs is also related to the possibility of tuning their properties to tailor a particular IL for a given end use. Most ILs of recent interest are based on nitrogen-rich alkylsubstituted heterocyclic cations, accompanied by different inorganic anions. By changing the lateral chain attached to the heterocyclic unit or the anion a wide variation in properties, such as viscosity, solvation, melting point, catalytic activity, can be obtained.[1–7] Alkylimidazolium halides ILs have been investigated by a variety of theoretical and experimental techniques, including X-ray diffraction,[8–11] Raman,[8,12] UV-Visible and Infrared,[13,14] extended X-ray absorption fine structure (EXAFS)[15–17] and X-ray absorption near edge structure (XANES)[18] spectroscopies, Car-Parrinello Molecular Dynamics[19] and classical Molecular Dynamics (MD)[9,12,16,20–23] simulations, and ab initio calculations.[13,24]

Despite this intense research activity a detailed characterization of the structural properties of alkylimidazolium halides is nowadays still lacking. In this framework, understanding how changes in the imidazolium lateral chain or in the anion can affect the short- and long-range structure of these materials represents a very important aspect that deserves further studies. Recently, XAS (X-ray absorption spectroscopy) has been used to investigate the local structure around the Br^- ion in 1-alkyl-3-methylimidazolium bromide ([$C_n$mim]Br) ILs with different alkyl chains (with n = 2, 4, 6, 8, 10), where the first two members of the series, namely [C_2mim]Br and [C_4mim]Br, are solid at room temperature, while the other compounds are liquid.[15] From the similarity of the XAS spec-

[a] *Dipartimento di Chimica, Università di Roma "La Sapienza", P.le A. Moro 5, 00185 Roma, Italy. E-mail: valentina.migliorati@uniroma1.it, p.dangelo@uniroma1.it.*
[b] *Elettra-Sincrotrone Trieste S.C.p.A s.s. 14, km 163.5, I-34149 Basovizza, Trieste, Italy*
[c] *European Synchrotron Radiation Facility, BP 220 38043, Grenoble Cedex, France*
† Electronic Supplementary Information (ESI) available: Tables S1-S2 and Figures S1-S4. See DOI: 10.1039/b000000x/

tra of [$C_n$mim]Br salts, from the butyl to the decyl derivatives, it was evinced that the molecular organization present in the [C_4mim]Br crystal phase is maintained also in the liquids at a local level, and the arrangement of the imidazolium head groups around the Br^- ion is the same independently from the length of the alkyl chain.[15] However, due to the short-range character of the XAS technique, no information could be obtained on the long-range structural changes that are expected to take place when the alkyl chain length of [$C_n$mim]Br ILs is modified.

The long-range organization and the existence of complex morphologies in ILs has been a topic of ongoing debate in the literature.[25–27] The formation of complex structures stems from the intrinsic amphiphilic nature of ILs and it is considered as one of the leading factor for many intriguing properties of this class of materials, including their ability to dissolve both polar and apolar compounds. Typical IL cations, such as alkylimidazolium, are characterized by a polar head bearing a positive charge, and an apolar alkyl tail: the interactions between the head groups and the anions are dominated by strong electrostatic forces, while the side chains interact mainly through weak short-range excluded volume interactions. According to several experimental and theoretical studies, the alkyl chains tend to segregate, thus leading to structural domains whose average size depends on the alkyl chain length.[25,28]

In addition to the lateral chain attached to the cation, the IL three-dimensional arrangements, and consequently many IL properties, are also influenced by the nature of the anion. Alkylimidazolium halides ILs containing the same cation and different halide ions can even show a different aggregation state, as in the case of 1-butyl-3-methylimidazolium iodide, [C_4mim]I, which is liquid at room temperature while the chloride and bromide analogous (i.e. [C_4mim]Cl and [C_4mim]Br) are solid. In a combined UV-Visible, Infrared spectroscopy and DFT study of liquid [C_4mim]I,[13] the difference between the melting points of these ILs has been ascribed to the formation of weaker hydrogen bonds between the most acidic ring proton of the imidazolium cation and the iodide ion. Moreover, by using MD simulations in combination with the Raman spectroscopy, Umebayashi and coworkers have found that in liquid [C_4mim]I the iodide ion has a lower probability of being located in front of the imidazolium ring proton as compared to [C_4mim]Cl and [C_4mim]Br.[12] However, no direct structural information on alkylimidazolium halides with different anions has been obtained thus far, due to the lack of experimental techniques able to provide such information and able to shed light on subtle structural changes that may take place going from one halide ion to another.

In this respect, EXAFS spectroscopy is the structural probe of choice, because of its intrinsic chemical specificity and short-range sensitivity.[29,30] However, in the case of disordered systems, the EXAFS data analysis can derive strong benefit from the use of structural results obtained from theoretical simulations as models in the analysis of the experimental data.[31–34] This is particularly true when dealing with alkylimidazolium halides ILs, in which the photoabsorber atom is surrounded by different light atoms such as carbon and nitrogen. From a theoretical point of view, classical MD simulations represent a valuable tool to investigate the structural properties of ILs and have been widely used to simulate ILs as pure liquids and in mixtures with other solvents.[9,20,35] Moreover, during the last years the synergic use of EXAFS and MD has been shown particularly well suited to obtain reliable structural information on disordered systems.[36,37]

Many important issues will be addressed. First, we will demonstrate that MD simulations are able to reproduce the existence of a local structural order around the Br^- ion that is the same independently from the length of the alkyl chain, as suggested by the XAS results reported in Ref[15]. On the other hand, use of MD simulations will allow us to study both the short- and long-range liquid structure, and to assess the effects of the alkyl chain length on the aggregation behavior of [$C_n$mim]Br ILs. Moreover, the synergic use of EXAFS and MD will allow us to obtain a thorough characterization of the local structure around the halide ion in [C_6mim]Br and [C_6mim]I and to shed light on similarities and differences in the three-dimensional arrangements of cations and anions in these two halide based ILs.

2 Methods

2.1 Molecular Dynamics Protocol

The MD simulations of liquid [$C_n$mim]Br (with n = 5, 6, 8, 10) and [C_6mim]I have been performed with the DL_POLY code.[38] As far as the interaction potentials are concerned, the Lopes and Pádua force field has been used for the $[C_n\text{mim}]^+$ cations and for Br^-,[39,40] while OPLS was employed for the I^- ion.[41] The Lorentz-Berthelot combining rules were employed in order to obtain Lennard-Jones parameters for all of the different atoms.

The simulations were carried out in the NVT ensemble, using the Nosé-Hoover thermostat[42,43] with a relaxation constant of 0.5 ps. The volume of the box has been chosen to reproduce the experimental density of the systems, with the exception of the [C_{10}mim]Br simulation in which the box edge length was obtained by equilibrating the system in the NPT ensemble at 1 atm and 300 K for about 5 ns. The initial configurations were constructed by randomly positioning the ions in a very large cubic simulation box, and, during the equilibration, a series of NPT runs at very high pressure (100 atm) were performed, to finally reach the system experimental density. Then, at the end of equilibration, a final NVT run at

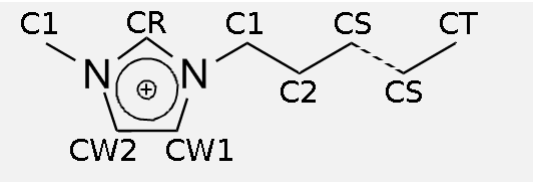

Fig. 1 Atom labeling used for the IL cations $[C_n mim]^+$. CS refers to the carbon atoms of the alkyl side chain that are located at least two bonds from the ring, so that $[C_n mim]^+$ cations with n = 5, 6, 8, 10 have 2, 3, 5 and 7 CS atoms, respectively.

300 K was performed for 10 ns. The production simulations were carried out for 10 ns, using a timestep of 1 fs and saving a configuration every 200 timesteps. The simulated cubic boxes were composed in all cases of 500 ion pairs and periodic boundary conditions were used to minimize edge effects. The box edge lengths employed were 53.53 Å, 55.05 Å, 58.02 Å, 61.28 Å, and 56.90 Å for $[C_5mim]Br$, $[C_6mim]Br$, $[C_8mim]Br$, $[C_{10}mim]Br$ and $[C_6mim]I$, respectively. Non-bonded interactions were treated using a cut-off distance of 15 Å, while for long-range electrostatic effects the Ewald summation method was employed.[44] The bonds involving hydrogen atoms were constrained with SHAKE.[45]

The structural properties of the investigated ILs have been described in terms of radial, combined and spatial distribution functions that have been calculated using the TRAVIS software.[46] Fig. 1 shows the atom labeling used in the paper to describe the structural results.

The X-ray structure factors $S(q)$ have been calculated from the MD simulations using the following equation:[47–49]

$$S(q) = \frac{\sum_{i=1}^{N}\sum_{j=1}^{N} x_i x_j f_i(q) f_j(q) H_{ij}(q)}{[\sum_{i=1}^{N} x_i f_i(q)]^2} \qquad (1)$$

where the indices i and j span the set of all atoms constituting the system, x_i and x_j are the fractions of atom species i and j, q is the momentum transfer, $f_i(q)$ and $f_j(q)$ are the atomic X-ray scattering factors of species i and j. $H_{ij}(q)$ are the partial structure factors, defined in terms of the radial distribution functions ($g_{ij}(r)$) by the Fourier integral:

$$H_{ij}(q) = 4\pi\rho_0 \int_0^{r_{max}} r^2 (g_{ij}(r) - 1) \frac{sin(qr)}{qr} dr \qquad (2)$$

where ρ_0 is the total number density of the system and r_{max} is the integration cutoff that is half the box edge. The X-ray structure factors have been computed using in-house written codes.

2.2 X-absorption measurements

$[C_n mim]Br$ (with n=5, 6, 8, 10) and $[C_6mim]I$ ILs were purchased from Iolitec GmbH with a stated purity of $> 99\%$. All ILs were dried in vacuum for about 48 h. The water content was then determined by Karl-Fischer titration and was found to be between 200 and 300 ppm for the different samples.

The Br K-edge XAS spectra of $[C_n mim]Br$ ILs were collected at RT in transmission mode at the ELETTRA Synchrotron (Trieste, Italy) on the beamline 11.1.[50] The monochromator was equipped with two flat Si111 crystals that were slightly detuned during data aquisition. The samples were placed in cells with Kapton windows and the thickness was adjusted to give an absorption change over the edge of about one logarithmic unit. To avoid contact with water the data acquisition was carried out keeping the cell under nitrogen flux. The storage ring was operating at 2 GeV with an optimal storage beam current between 300 and 130 mA.

The I K-edge XAS spectrum of $[C_6mim]I$ was collected in transmission mode at RT at the BM23 beamline of the European Synchrotron Radiation Facility ESRF. The monochromator was equipped with two flat Si311 crystals and to reduce harmonic contamination the crystals were kept slightly detuned with a feedback system. The storage ring was operating at 2 GeV with a beam current of 310 mA. Measurements of liquid $[C_6mim]I$ were carried out with a cell with Kapton windows and a Teflon spacer of 1 mm under nitrogen flux.

2.3 EXAFS data analysis

The EXAFS data analysis has been performed using the GNXAS program and the theoretical framework of the method is described in detail in previous publications.[51,52]

Due to the structural disorder and to the high number of scattering atoms contributing to the total $\chi(k)$ signal, rather than using the usual discrete form of the EXAFS equation, the signal is modelled as a function of the radial distribution function $g(r)$ as:

$$\chi(k) = \int_0^{\infty} dr\, 4\pi\rho r^2 g(r) A(k,r) \sin[2kr + \phi(k,r)] \qquad (3)$$

where $A(k,r)$ and $\phi(k,r)$ are the amplitude and phase functions, respectively, and ρ is the density of the scattering atoms. $\chi(k)$ theoretical signals are calculated by introducing the MD $g(r)$'s in eqn (3) and the comparison between the experimental and theoretical curves allows one to assess the reliability of theoretical framework used in the simulations.

In particular, theoretical $\chi(k)$ signals have been calculated both for bromide and iodide ILs using the MD X-HCR, X-HCW, X-H1, X-H2, X-CR, X-CW, X-C1, X-N and X-C2 $g(r)$'s obtained from the simulations (X is Br and I). The contribution associated with the C2 and N atoms has been ne-

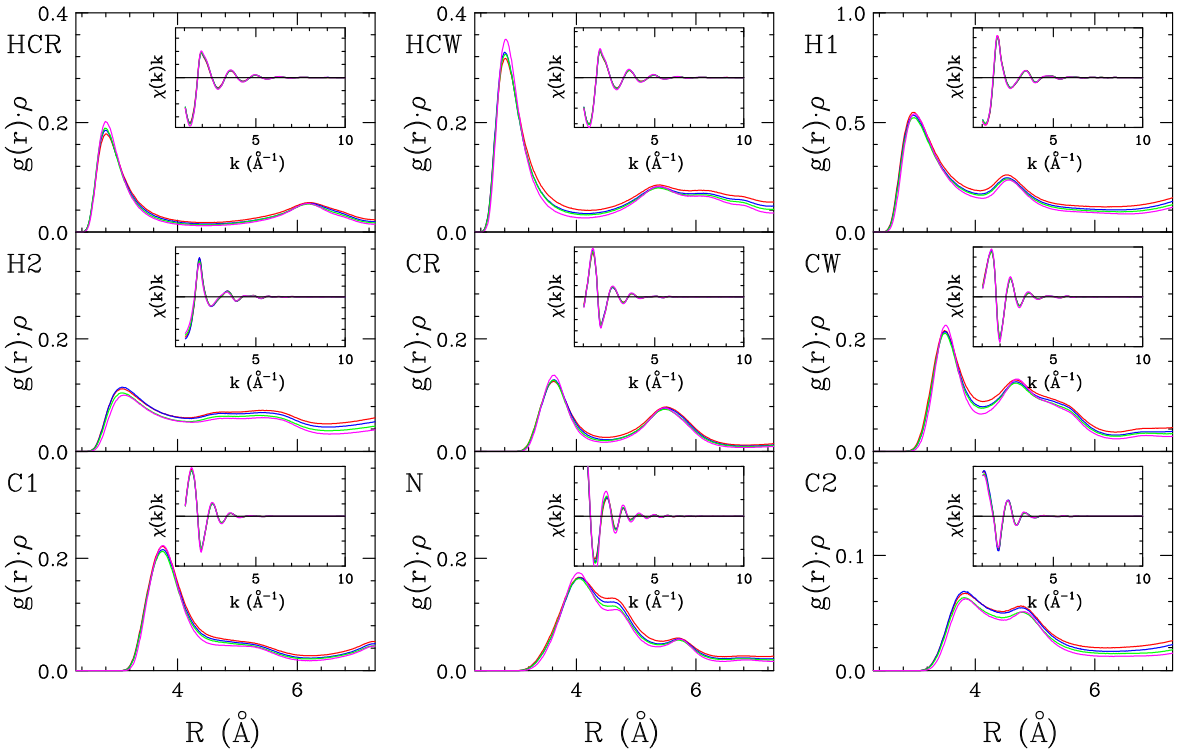

Fig. 2 Br-Y radial distribution functions, $g(r)$'s, multiplied by the numerical density of the observed atoms Y (ρ), calculated from the MD simulations of [C_5mim]Br (red), [C_6mim]Br (blue), [C_8mim]Br (green) and [C_{10}mim]Br (magenta). The corresponding theoretical χ(k) signals calculated from the MD $g(r)$'s are shown in the insets.

glected in the case of [C_6mim]I, as the amplitude of the theoretical signals is very low. During the minimization procedure only two non structural parameters, namely the ionization threshold energy E_0 and S_0^2, are optimized.

3 Results

3.1 Local order around the Br^- ion in [$C_n$mim]Br ILs

In a previous investigation it has been shown that the XANES spectra of the [$C_n$mim]Br ILs are identical from the butyl to the decyl derivative, thus meaning that the local structure around the Br^- ion is the same independently from the length of the alkyl chain.[15] This result is quite unexpected as the length of the alkyl chain will certainly influence the structural organization in the long-range regions. In the first step of this investigation we have calculated the $g(r)$'s involving the Br^- ion from the MD trajectories of all the [$C_n$mim]Br ILs and the results obtained for [C_6mim]Br IL are reported in Fig. S2 of ESI† as an example. In order to make a comparison among different ILs having different densities, in Fig. 2 we report all of the $g(r)$'s multiplied by the numerical density. Starting from the MD $g(r)$'s we have calculated the χ(k) theoretical signals associated with all the atoms surrounding the photoabsorber up to a cut-off distance of 4.0 Å using eqn (3). We have checked that the amplitude of the signals associated with higher distance shells is negligible. The comparison among the $g(r)$'s and theoretical χ(k) signals is shown in Fig. 2; the $g(r)$'s are very similar for all the ILs, while the EXAFS curves are identical. This finding is in agreement with previous XANES results[15] and indicates that the local structure of the Br^- ion is not influenced by the alkyl chain.

In the second step the Br K-edge experimental EXAFS spectra of liquid [$C_n$mim]Br have been analyzed using the MD $g(r)$'s. Note that a direct comparison between the local structure around the Br^- ion obtained from the MD calculations and the EXAFS data allows a proper interpretation of the experimental spectra on the one hand, and the assessment of the reliability of the simulations on the other. EXAFS theoretical spectra have been calculated by adding all the χ(k) curves reported in Fig. 2. Least-squares fits of the EXAFS spectra have been carried out in the range k = 2.0-9.3 $Å^{-1}$ keeping fixed the MD structural parameters and optimizing the non structural parameters to improve, as far as possible, the agreement

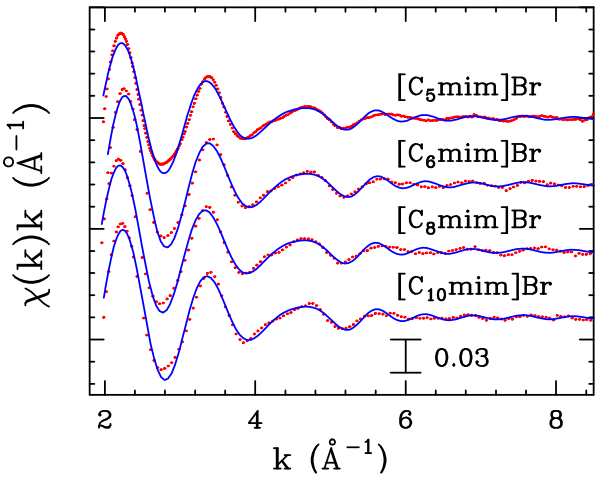

Fig. 3 Comparison between the EXAFS experimental spectra (red dotted line) and the theoretical signals calculated from the MD simulations of [C$_n$mim]Br ILs (solid blue lines).

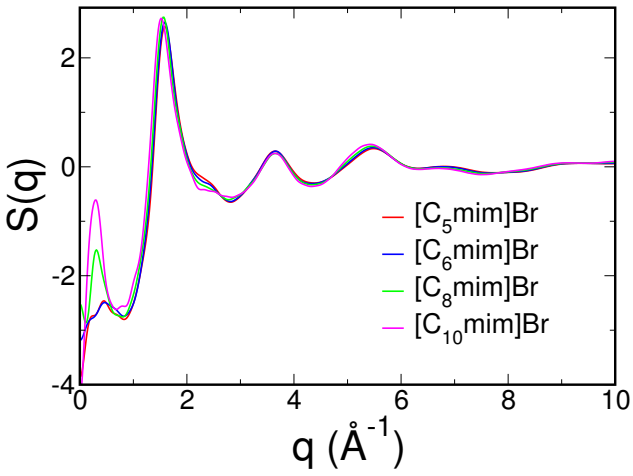

Fig. 4 X-ray structure factors $S(q)$ calculated from the MD simulations of [C$_n$mim]Br ILs.

between theoretical and experimental spectra. The best-fit results are shown in Fig. 3; the agreement between theory and experiment is quite good in all cases demonstrating the validity of the overall procedure. From the EXAFS analyses E_0 was found to be 1 eV above the first inflection point of the spectrum, while S_0^2 was found to be 0.85, in all cases.

3.2 Long-range organization in [C$_n$mim]Br ILs

The very interesting result of the EXAFS experiments combined with MD simulations is that the arrangement of the imidazolium head groups around the Br^- ion in liquid [C$_n$mim]Br ILs (with n = 5, 6, 8, 10) is the same independently from the length of the alkyl chain. However, due to the short-range character of the EXAFS technique, no information can be obtained from the EXAFS experimental data about the long-range structural changes that are expected to take place when the alkyl chain length of [C$_n$mim]Br ILs is modified. Conversely, from the analysis of the MD trajectories it is possible to provide a global picture of the structural properties of condensed-phase materials, both in the short- and long-distance range. In order to investigate the long-range organization and tail aggregation phenomenon in [C$_n$mim]Br ILs it is useful to calculate theoretical X-ray structure factors $S(q)$ starting from the MD $g(r)'s$ using eqns (1) and (2).

Fig. 4 shows the $S(q)$ calculated from the MD simulations of [C$_5$mim]Br, [C$_6$mim]Br, [C$_8$mim]Br and [C$_{10}$mim]Br. Above 1 Å^{-1}, all of the $S(q)$ show a very similar trend: they are characterized by a principal peak at 1.50-1.60 Å^{-1}, followed by two less intense peaks centered at 3.65 and 5.50 Å^{-1}, and some less defined oscillations beyond this q range. These features are mostly due to intramolecular contributions, as well as to intermolecular short-range interactions; the similarity among the structure factors of all the investigated ILs in the q region above 1 Å^{-1} is in line with our result that cations and anions in [C$_n$mim]Br ILs are involved in a network of short-range interactions whose pattern is the same regardless the alkyl chain length. Conversely, remarkable differences are found in the q range below 1 Å^{-1}. The first important result is the presence, for all the [C$_n$mim]Br ILs, of the so-called prepeak, that is a peak located at low q values which is the fingerprint for the occurrence of long-range structural correlations. Both the prepeak intensity and position strongly depend on the length of the alkyl chain: the intensity becomes higher and the prepeak shifts towards shorter q values as the alkyl chain attached to the $[C_n mim]^+$ cation becomes longer. In particular, the prepeak maxima are found at q values of 0.45 Å^{-1} for [C$_5$mim]Br and [C$_6$mim]Br, 0.31 Å^{-1} for [C$_8$mim]Br and 0.30 Å^{-1} for [C$_{10}$mim]Br. The prepeak position obtained for [C$_8$mim]Br is in very good agreement with the large angle X-ray scattering experimental data reported in a combined X-ray diffraction and MD study on [C$_8$mim]Cl and [C$_8$mim]Br.[9] It is important to point out that the MD simulation of [C$_8$mim]Br carried out in Ref.[9] was not able to reproduce the presence of the peak at low q values evidenced from the X-ray scattering experiments. This is probably due to the use of the Debye's scattering equation to compute the theoretical $S(q)$ function from the MD trajectories, instead of calculating the radial distribution functions among all of the atoms and using eqns (1) and (2). Similar trends of the $S(q)$ prepeak upon alkyl chain elongation have been previously obtained for imidazolium-based ILs with different anions both experimentally and theoretically.[22,25–27] To

interpret the observed structural dependency of the prepeak on alkyl tail length, different ideas have been proposed in the literature. According to some authors this peak is due to cationic tail interdigitation, to the formation of micelles, strands, and other more complex morphologies even in the case of imidazolium systems with modest tail lengths such as $[C_5mim]^+$.[53,54] However, recent works by Hardacre et al. and by Margulis et al. have suggested that the prepeak is a simple consequence of cationic anisotropy, which imposes certain patterns of coordination along the direction of the longer alkyl tail and it is not due to complex long-range morphologies.[26,27] In these studies the existence of complex morphologies in ILs was neither proved nor disproved, but it has been shown that the prepeak can be explained by much simpler considerations of solvation shell asymmetry as it emerges as a consequence of scattering contributions of the imidazolium head and not of the alkyl tails.[26,27] Understanding the precise origin of the prepeak in the X-ray structure factors of imidazolium based ILs is beyond the scope of the present paper; however, as a matter of fact, the presence of a prepeak in the $S(q)$ function indicates the existence of long-range structural correlations that are strengthened and are related to longer distances with increasing length of the alkyl substituents. Due to the intrinsic amphiphilic nature of ILs the apolar alkyl tails tend to aggregate in $[C_nmim]Br$ ILs, while a tridimensional network of ionic channels is formed by anions and imidazolium head groups. In order to gain visual insights into this behavior, we report in Fig. 5 representative MD snapshots of the simulation boxes of $[C_nmim]Br$ ILs in which the polar heads and the alkyl chains of the imidazolium cations are colored magenta and azure, respectively. The presence of hydrophilic channels crossing the box are clearly visible as white regions in the right panels of the figure where only the hydrophobic portions of the systems are shown for better visualization. As the length of the alkyl chain increases, the nonpolar aggregates become larger and more connected producing larger and larger separations among the polar box regions dominated by strong electrostatic forces.

3.3 Influence of the anion on the IL structure: $[C_6mim]Br$ versus $[C_6mim]I$

The results of our MD simulations of $[C_nmim]Br$ (with n = 5, 6, 8, 10) used in conjunction with the EXAFS experimental data have revealed that the length of the alkyl chain attached to the imidazolium cation does not alter the local arrangement of cations around the Br^- ions, while having an effect on the long-range organization of these materials. We are now interested in understanding how cation-anion interactions in alkylimidazolium halides are influenced by the nature of the anion. To this end we have decided to study two alkylimidazolium halides having the same alkyl substituent

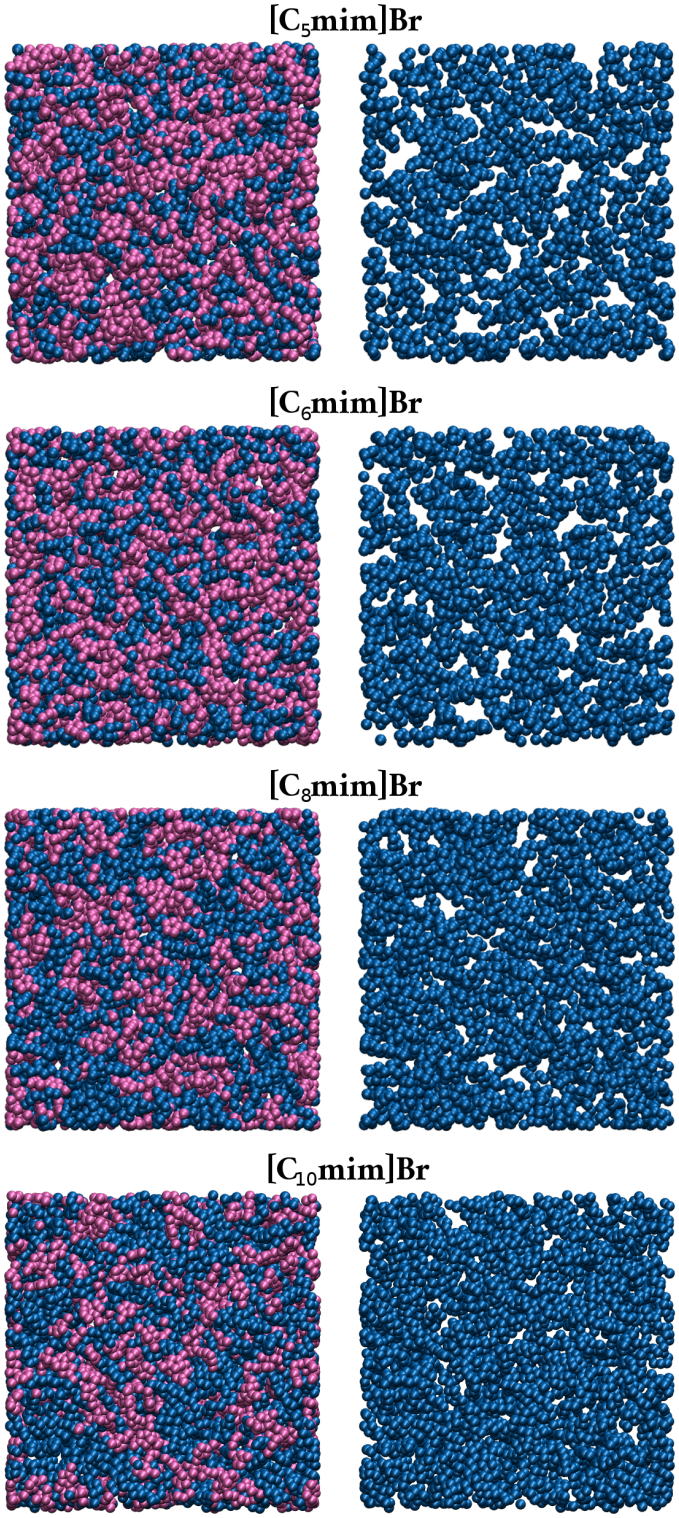

Fig. 5 Snapshots of MD simulation boxes of $[C_nmim]Br$ ILs where the polar heads and the alkyl chains of the imidazolium cations are colored magenta and azure, respectively. In the right panels only the hydrophobic portions of the systems are shown for better visualization.

(C_6) and two different halide ions: Br^- and I^-. It is important to stress that due to existence of similar arrangements of cations and anions at a local level in [$C_n$mim]Br (with n = 5, 6, 8, 10), the description of short-range cation-anion interactions obtained for [C_6mim]Br can be reasonably extended to [C_5mim]Br, [C_8mim]Br and [C_{10}mim]Br.

Radial distribution functions. In order to investigate the structural properties of [C_6mim]Br and [C_6mim]I and to shed light on similarities and differences in the arrangements of cations and anions in these halide based ILs, it is useful to calculate from the MD trajectories the radial distribution functions $g(r)$'s among selected atoms of the systems. The calculated $g(r)$'s are shown in Fig. 6, while Tables S1 and S2 of ESI† report the $g(r)$ structural parameters obtained for [C_6mim]Br and [C_6mim]I, respectively: first peak distances, coordination numbers calculated by integrating the $g(r)$'s up to the first minimum, cutoff distances used in the calculation of the coordination numbers. The $g(r)$'s between the halide ion (X) and the imidazolium ring center (Cation) are depicted in the upper panel of Fig. 6. Note that throughout the paper the imidazolium ring center indicates the ring geometrical center of the imidazolium cation and not the center of mass. The X-Cation $g(r)$'s exhibit a distinct first peak indicating the existence of a well-defined first coordination shell both in [C_6mim]Br and [C_6mim]I. The X-Cation first shell distances becomes longer going from Br^- to I^-, as expected, and the number of cations surrounding the halide ion in the first coordination sphere increases (see Tables S1 and S2 of ESI†).

The atoms of the $[C_6mim]^+$ cation that form the strongest interactions with the halide ion are the three hydrogen atoms of the imidazolium ring plane, HCR and the two HCWs. The X-HCR and X-HCWs $g(r)$'s are depicted in the middle and lower panels of Fig. 6, respectively. All of the calculated $g(r)$'s show a sharp first peak, followed by other less intense peaks, and, also in this case, the $g(r)$'s involving the I^- ion are shifted towards larger distances as compared to the Br^- functions. It is useful to compare the behavior of the three $g(r)$'s within the same IL, and in both cases the same general trend is observed: the intensity of the X-HCR $g(r)$ first peak is slightly higher and the peak is more structured as compared to the X-HCW $g(r)$ first peak, suggesting that the interaction of the halide ion with HCR is stronger, being HCR the most acidic hydrogen atom of the imidazolium cation. On the other hand, the X-HCR, X-HCW1 and X-HCW2 first shell distances are very similar to each other, while the coordination numbers are slightly different, also as a consequence of the different cutoff values used in the calculation (see Tables S1 and S2 of ESI†). Moreover, the X-HCW1 and X-HCW2 $g(r)$'s are practically coincident at low distances and show some differences in the longer distance range. It is important to stress that the presence of a second peak in the halide-hydrogen $g(r)$'s, which is more defined in the X-HCR $g(r)$ and oscillating in

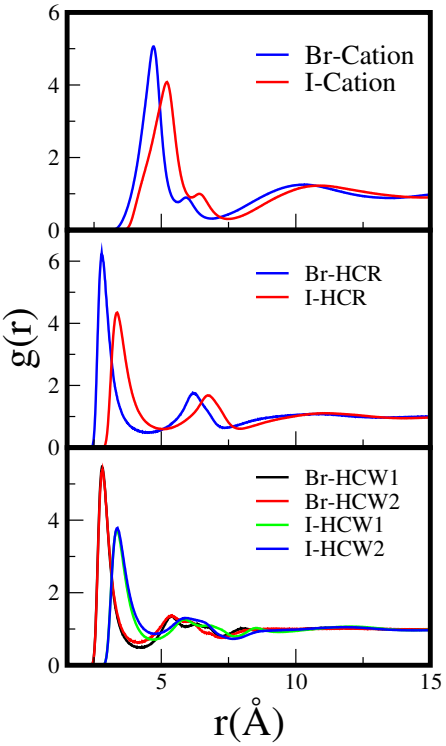

Fig. 6 Radial distribution functions, $g(r)$'s, calculated from the MD simulations of [C_6mim]Br and [C_6mim]I. Top panel: X-Cation $g(r)$'s calculated between the ring center of the $[C_6mim]^+$ cation and the X^- ion. Central panel: X-HCR $g(r)$'s. Bottom panel: X-HCW1 and X-HCW2 $g(r)$'s.

the X-HCW1 and X-HCW2 $g(r)$'s, is not to be interpreted as a second shell interaction. Indeed, it is due to the presence of halide ions interacting with hydrogen atoms on the opposite side of the imidazolium cation with respect to the hydrogen atom used in the $g(r)$ calculation. As mentioned above, from the analysis of the X-Cation $g(r)$, it has been possible to obtain the average number of cations surrounding the halide ion in its first coordination shell. In order to investigate how the anion-cation coordination numbers vary along the MD trajectories, we have defined an instantaneous coordination number (n) using the same cutoff value as before (Tables S1 and S2 of ESI†) to define the X-Cation first coordination shell, and we have calculated the instantaneous coordination number distribution expressed in percentage (see Fig. S1 of ESI†.). In both [C_6mim]Br and [C_6mim]I a dominant percentage of anions are coordinated by four cations, and vice versa. However, the Br-Cation and I-Cation coordination number can take all values from 2 to 6, and in the I^- case the distribution is shifted towards larger n values: the second favored configuration is a 3-coordinated and a 5-coordinated species in [C_6mim]Br and [C_6mim]I, respectively.

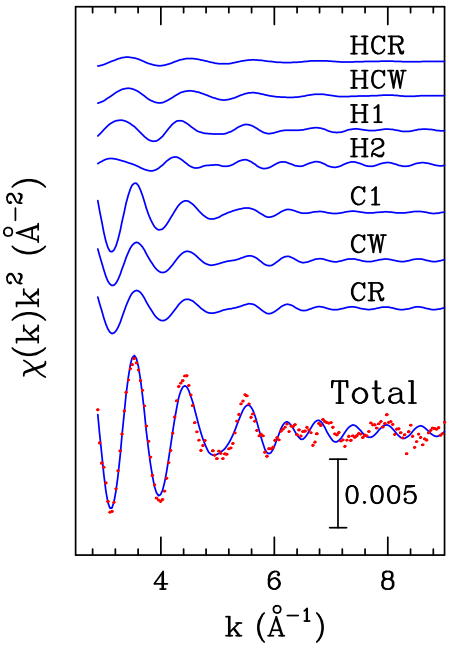

Fig. 7 Comparison between the EXAFS experimental data (dotted red line) of [C_6mim]I and the theoretical signal calculated from the I-HCR, I-HCW, I-H1, I-H2, I-C1, I-CW and I-CR MD $g(r)$'s (solid blue line).

EXAFS analysis of [C_6mim]I. As previously done for the [$C_n$mim]Br ILs, in order to assess the validity of structural results obtained from the MD simulation, we have directly compared the EXAFS experimental data with the $g(r)$'s involving the I^- ion for [C_6mim]I (see Fig. S3 of ESI†).

When comparing the Br^- and I^- $g(r)$'s shown in Fig. S2 and S3 of ESI† it appears that the former ion coordinates the imidazolium cation at shorter distances as compared to the latter. This behavior is not surprising considering the ionic radii of the two ions, but this strongly influences the amplitude of the EXAFS signal. The I-C2 and I-N $g(r)$'s of [C_6mim]I are above 4 Å and these atoms provide a negligible contribution to the EXAFS spectrum. For this reason only the I-HCR, I-HCW, I-H1, I-H2, I-C1, I-CW and I-CR χ(k) signals have been included in the data analysis and the best fit results are shown in Fig. 7. Also in this case the structural parameters have been kept fixed to those obtained from the MD simulations and only the non structural parameters have been refined. As evident from Fig. 7 the agreement between the experimental and theoretical spectra is good also if for k values higher than 7 $Å^{-1}$ the signal to noise ratio is quite low. This is due, as previously mentioned, to the very low amplitude of the scattering signal of the hydrogen and carbon atoms that are quite distant from the I^- ion. The minimization has been carried out in the k range between 3.0 and 9.2 $Å^{-1}$ and E_0 has been found 8 eV above the first inflection point of the spectrum while S_0^2 is 0.9. Also in this case the agreement between the MD and EXAFS data proves the substantial correctness of the structural results obtained from the simulation.

Combined distribution functions. Once the validity of the MD structural results have been assessed for both [C_6mim]Br and [C_6mim]I ILs, additional insights into the three-dimensional arrangement of the ions can be gained by analyzing combined radial/angular distribution functions (CDFs) from the MD trajectories. In this analysis distances and angles stemming from a MD configuration are regarded as a 2-tuple and a two-dimensional histogram showing their correlation is computed. In particular, we have calculated the CDF between the HCR-X $g(r)$ and the distribution function of the angle (ω_{HCR}) formed between the CR-HCR and CR-X directions (see Fig. S4 of ESI† for angle definition). In order to study also the interactions between the halide ion and the other two ring protons (HCW1 and HCW2), we have combined the HCW-X $g(r)$ and the distribution function of the angle formed between the CW-HCW and CW-X directions. The CDFs calculated from the MD simulation of [C_6mim]Br are depicted in the left panels of Fig. 8. As concerns the HCR atom, the CDF (panel A) shows a region of maximum intensity for a distance of about 2.8 Å and angles between 20° and 40°, meaning that the Br^- ion prefers to form an angle of about 30° with the CR-HCR direction rather than being located in front of the CR-HCR vector. A similar result has been obtained from the CDF pertaining to the HCW2 atom (panel E), as also in this case the Br^- ion has a tendency to be tilted of about 30° with respect to the CW2-HCW2 vector. Conversely, the CDF for the HCW1 atom shows a larger region of maximum intensity as compared to the other two CDFs, ranging from 0° to 30° at a distance of 2.8 Å. This can be due to the steric hindrance of the hexyl chain near the HCW1 atom that forces the Br^- ion towards the CW1-HCW1 direction. Right panels of Fig. 8 depict the CDFs calculated for liquid [C_6mim]I. As it can be seen, all of the CDF concerning the I^- ion show a much lower intensity as compared to the Br^- counterparts, meaning that the radial/angular correlation is lower due to the weaker interactions formed between I^- and the imidazolium ring protons. On the other hand, the general trend of the CDFs is very similar to the one obtained for the Br^- ion: the regions of highest intensity are found at longer distances (at about 3.3 Å), as expected, but the angles are comparable. Therefore, both the halide ions arrange in a similar way with respect to the directions of the C-H bonds of the imidazolium ring plane.

As it is not possible to establish the position of the halide ions with respect to the imidazolium ring plane from the latter analysis, we have also calculated CDFs combining the H-X $g(r)$ (where H=HCR, HCW1 and HCW2) and the distribution function of the angle (θ) formed between the normal

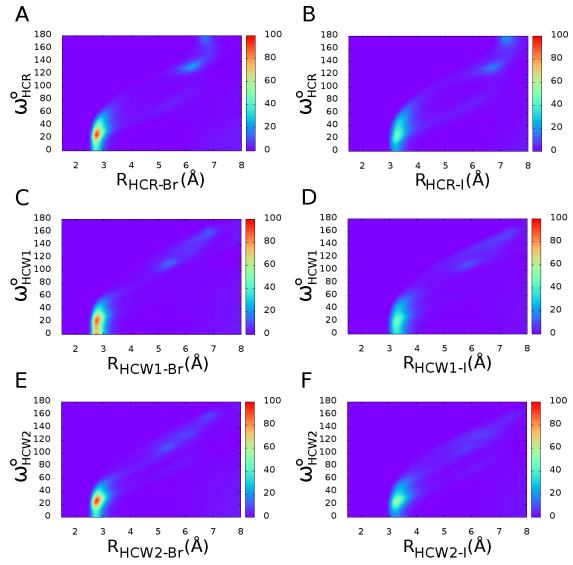

Fig. 8 Combined distribution functions (CDFs) calculated from the MD simulations of [C_6mim]Br (left panels) and [C_6mim]I (right panels). The CDFs show the correlation between the H-X $g(r)$ (x-axis) and ADF of the angle between the C-H and C-X vectors (y-axis). (A and B) CDFs calculated for the HCR atom. (C and D) CDFs calculated for the HCW1 atom. (E and F) CDFs calculated for the HCW2 atom.

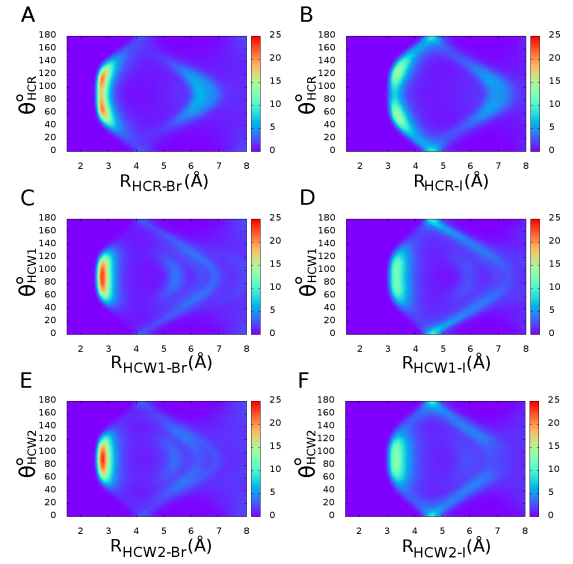

Fig. 9 Combined distribution functions (CDFs) calculated from the MD simulations of [C_6mim]Br (left panels) and [C_6mim]I (right panels). The CDFs show the correlation between the H-X $g(r)$ (x-axis) and ADF of the angle between the normal vector to the ring plane and the ring center-X vector (y-axis). (A and B) CDFs calculated for the HCR atom. (C and D) CDFs calculated for the HCW1 atom. (E and F) CDFs calculated for the HCW2 atom.

vector to the ring plane and the ring center-X vector (see Fig. S4 of ESI† for angle definition). The CDFs calculated for the HCR, HCW1 and HCW2 ring proton of [C_6mim]Br are shown in panels A, C and E of Fig. 9, respectively. As far as the HCR atom is concerned, a high intensity region has been obtained for all angles comprised between 60° and 120°. In the case of HCW1 and HCW2, the CDFs are very similar to each other and show the highest correlation for angles comprised between 70° and 110°, indicating that the Br^- ion is more likely to form lower angles with the ring plane when interacting with HCW1 and HCW2. Panels B, D and F of Fig. 9 depict the CDFs calculated from the MD trajectory of [C_6mim]I (for HCR, HCW1 and HCW2, respectively). All of the CDFs for the I^- ion have lower intensity as compared to the Br^- ones, as previously observed for the CDFs involving the ω angle, while a different trend of the CDFs is found for the two halide ions. In the case of I^-, the CDF concerning the HCR-I interactions shows two high intensity regions (the first comprised between 40° and 70°, and the latter between 110° and 140°), and a low intensity region around 90°: the I^- ion has the tendency to be positioned above and below the ring plane and not coplanar with it. Conversely, when interacting with either HCW1 or HCW2, I^- has a similar probability of being coplanar with the ring plane or to form with the plane itself angles up to about 20°.

Spatial distribution functions. The three-dimensional organization of the halide ions around the $[C_6mim]^+$ cation can be observed looking at the spatial distribution functions (SDFs) depicted in Fig. 10. In order to properly compare the SDFs obtained for [C_6mim]Br and [C_6mim]I, we have shown the SDFs using the same absolute densities for both systems. It is seen that the favorite sites of interactions of both halide ions are the three hydrogen atoms of the imidazolium ring, as expected. An interesting result that emerges from the SDF analysis is the different spatial arrangement of the Br^- and I^- ions in the vicinity of the HCR atom: I^- prefers to be above and below the imidazolium ring plane and not coplanar with the plane itself. Conversely, the Br^- ion has a high probability also to be located in the ring plane. Beside this difference, a similar three-dimensional organization of the halide ions around the cations has been obtained: the X^- distributions near HCR are broader as compared to the distributions near HCWs, and the X^- ions interacting with HCR can reach regions of space near the normal vector to the ring plane that are inaccessible to the anions in the vicinity of HCWs, in line with the results obtained from the CDF analysis. Moreover, both Br^- and I^- show a different arrangement in proximity of HCW1 and HCW2: near HCW2 the isosurfaces are shifted towards the methyl group, while near HCW1 the steric hindrance of the hexyl lateral chain hinders the approach of the halide ion.

It is interesting to compare our structural results found for alkylimidazolium ILs based on the Br^- and I^- ions with the

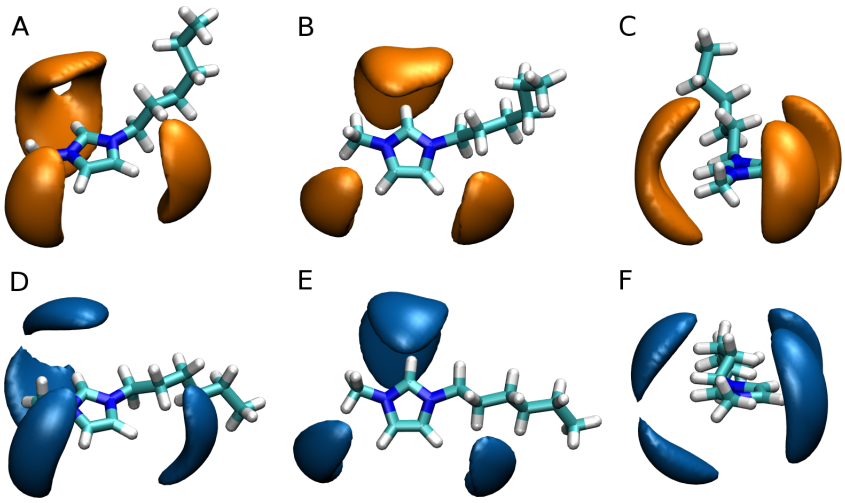

Fig. 10 Spatial distribution functions (SDFs) of the Br^- ion (orange) and the I^- ion (blue) around the $[C_6mim]^+$ cation, calculated from the MD simulations of $[C_6mim]Br$ (panels A, B and C) and $[C_6mim]I$ (panels D, E and F). Three different orientations have been shown for each system.

results previously obtained from MD investigations of their chlorinated counterparts.[55–59] In particular, the spatial distribution functions of the Cl^- ions around the imidazolium cations have been calculated in several studies,[55–59] showing that the Cl^- ions cluster around the positively charged hydrogen atoms of the cation ring. The cation-anion three-dimensional arrangements reported in the literature for Cl^- are very similar to the ones obtained in the case of the Br^- ion, while showing some differences with I^-. As mentioned above, in the I^- case the halide population facing the HCR atom decreases and it is compensated by an increase of the population above and below the ring plane. The different behaviour of Cl^- and Br^- as compared to I^- can be explained on the basis of their different ionic radii: the smaller Cl^- and Br^- anions tend to be located in the plane, while the larger I^- ion does not fit well in the imidazolium plane and it prefers to be either below or above it.

3.4 Conclusions

In this work, a thorough characterization of the structural properties of alkylimidazolium halides ILs, namely $[C_nmim]Br$ with n = 5, 6, 8, 10 and $[C_6mim]I$, has been carried out by combining MD simulations and EXAFS spectroscopy, with the aim of elucidating the structural changes that take place in alkylimidazolium halides when either the alkyl chain or the halide ion is modified.

The first important result of this work is that the arrangement of the imidazolium head groups around the Br^- ion in liquid $[C_nmim]Br$ ILs (with n = 5, 6, 8, 10) is almost the same, independently from the length of the alkyl chain. This implies that in $[C_nmim]Br$ ILs local ordered structures exist, in which anions and charge-bearing imidazolium heads interact with each other through strong Coulomb attraction and form a local three-dimensional bonding pattern that is common to all the $[C_nmim]Br$ IL family. The existence of local structures in $[C_nmim]X$ ILs has been previously suggested in the literature[60] and here, for the first time, it has been demonstrated by using an experimental technique that directly probes the local structure around the Br^- ion, in conjunction with MD simulations. The same pattern of cation-anion local interactions is found also in solid $[C_4mim]Br$, as evidenced in a recent XAS investigation of $[C_nmim]Br$ salts.[15]

Even if the local molecular organization around the Br^- ion is preserved, significant long-range structural changes take place when the alkyl chain length of $[C_nmim]Br$ ILs is modified. In order to investigate the long-range organization of $[C_nmim]Br$ theoretical X-ray structure factors have been calculated starting from the MD simulations and a low q peak has been found for all of the investigated ILs. This low q peak indicates the existence of long-range structural correlations and it moves to longer distances, increases in intensity and sharpens with increasing alkyl chain length on the cation. Due to the intrinsic amphiphilic nature of ILs, the apolar alkyl tails tend to aggregate in $[C_nmim]Br$ ILs, while a tridimensional network of ionic channels is formed by anions and imidazolium head groups.

While the alkyl chain attached to the imidazolium cation does not alter the local arrangement of cations around the Br^- ions, significant differences in the cation-anion local coordination have been found varying the IL anion. In order to

understand how cation-anion interactions in alkylimidazolium halides are influenced by the nature of the anion, we have carried out a thorough characterization of the structural properties of two alkylimidazolium halides having the same alkyl substituent and two different halide ions: $[C_6mim]Br$ and $[C_6mim]I$. A well defined first coordination shell of X^- ions around the imidazolium cation has been found from the analysis of the MD trajectories for both ILs. This coordination shell is composed on average by 3.7 and 4.2 X^- ions in $[C_6mim]Br$ and $[C_6mim]I$, respectively, even if instantaneously the cation-anion coordination number can take a value in the range between 2 and 6. The favorite sites of interactions of both halide ions are the three hydrogen atoms of the imidazolium ring, and a very interesting result that emerged from our investigation is the different spatial arrangement of the Br^- and I^- ions in the vicinity of the more acidic hydrogen atom of the imidazolium ring plane: I^- prefers to be above and below the ring plane and not coplanar with the plane itself. Conversely, the Br^- ion has an high probability also to be located in the ring plane.

In this work we have carried out the quantitative analysis of the Br and I K-edge EXAFS spectra of alkylimidazolium halides ILs, starting from the microscopic description of the systems derived from MD simulations. The very good agreement between theory and experiment that we obtained for all investigated systems ensures that the chosen force fields are able to provide a correct description of the local structural environment seen by the halide ion in alkylimidazolium halides ILs. This result is very important as the combined use of EXAFS and MD represents a very strict test of the force field quality, and, without such a comparison, the reliability of the theoretical structural results obtained from the simulations is hardly provable.

In conclusion, the combined MD and EXAFS approach used here enabled us to gain a clear picture of the structural properties of alkylimidazolium halides and to shed light on both the short- and long-range structural changes that take place in alkylimidazolium halides when either the alkyl chain or the halide ion is modified. All together these issues are expected to be of great help in the systematic design of IL systems to meet the requirements of key applications.

Acknowledgments

We would like to thank Alessandra Olarini for her invaluable help. This work was supported by the University of Rome "La Sapienza" (Progetto ateneo 2014, n.C26A14L7CX) and by the CINECA supercomputing centers through the grant IsC23_GEDI (n.HP10CLG9ZC).

References

1 M. Freemantle, *An Introduction to Ionic Liquids*, RSC Publishing, 2009.
2 *Ionic Liquids IIIA: Fundamentals, Progress, Challenges, and Opportunities: Properties and Structure*, ed. R. Rogers and K. Seddon, American Chemical Society, Washington D.C., 2005, vol. 901.
3 V. Migliorati, P. Ballirano, L. Gontrani, A. Triolo and R. Caminiti, *J. Phys. Chem. B*, 2011, **115**, 4887–4899.
4 *Ionic Liquids IIIB: Fundamentals, Progress, Challenges, and Opportunities: Transformations and Processes*, ed. R. Rogers and K. Seddon, American Chemical Society, Washington D.C., 2005, vol. 902.
5 V. Migliorati, P. Ballirano, L. Gontrani and R. Caminiti, *J. Phys. Chem. B*, 2012, **116**, 2104–2113.
6 R. D. Rogers and K. R. Seddon, *Science*, 2003, **302**, 792–793.
7 L. Gontrani, E. Bodo, A. Triolo, F. Leonelli, P. D'Angelo, V. Migliorati and R. Caminiti, *J. Phys. Chem. B*, 2012, **116**, 13024–13032.
8 H. Katayanagi, S. Hayashi, H. Hamaguchi and K. Nishikawa, *Chem. Phys. Lett.*, 2004, **392**, 460–464.
9 E. Bodo, L. Gontrani, A. Triolo and R. Caminiti, *J. Phys. Chem. Lett.*, 2010, **1**, 1095–1100.
10 B. Aoun, A. Goldbach, S. Kohara, J.-F. Wax, M. A. González and M.-L. Saboungi, *J. Phys. Chem. B*, 2010, **114**, 12623–12628.
11 A. E. Bradley, C. Hardacre, J. D. Holbrey, S. Johnston, S. E. J. McMath and M. Nieuwenhuyzen, *Chem. Mater.*, 2002, **14**, 629–635.
12 Y. Umebayashi, H. Hamano, S. Tsuzuki, J. N. Canongia Lopes, A. A. H. Pádua, Y. Kameda, S. Kohara, T. Yamaguchi, K. Fujii and S.-i. Ishiguro, *J. Phys. Chem. B*, 2010, **114**, 11715–11724.
13 M. Shukla, N. Srivastava and S. Saha, *J. Mol. Struct.*, 2010, **975**, 349–356.
14 R. Katoh, M. Hara and S. Tsuzuki, *J. Phys. Chem. B*, 2008, **112**, 15426–15430.
15 P. D'Angelo, A. Zitolo, V. Migliorati, E. Bodo, G. Aquilanti, J. L. Hazemann, D. Testemale, G. Mancini and R. Caminiti, *J. Chem. Phys.*, 2011, **135**, 074505.
16 V. Migliorati, A. Serva, G. Aquilanti, L. Olivi, S. Pascarelli, O. Mathon and P. D'Angelo, *Phys. Chem. Chem. Phys.*, 2015, **17**, 2464–2474.
17 P. D'Angelo, A. Zitolo, G. Aquilanti and V. Migliorati, *J. Phys. Chem. B*, 2012.
18 A. Zitolo, V. Migliorati, G. Aquilanti and P. D'Angelo, *Chem. Phys. Lett.*, 2014, **591**, 32–36.
19 M. H. Ghatee and Y. Ansari, *J. Chem. Phys.*, 2007, **126**, 154502.
20 M. H. Ghatee, A. R. Zolghadr, F. Moosavi and Y. Ansari, *J. Chem. Phys.*, 2012, **136**, 124706.
21 S. Yeganegi, V. Sokhanvarana and A. Soltanabadi, *Mol. Sim.*, 2013, **39**, 1070–1078.
22 S. M. Urahata and M. C. C. Ribeiro, *J. Chem. Phys.*, 2004, **120**, 1855–1863.
23 M. Kohagen, M. Brehm, Y. Lingscheid, R. Giernoth, J. Sangoro, F. Kremer, S. Naumov, C. Iacob, J. Kärger, R. Valiullin and B. Kirchner, *J. Phys. Chem. B*, 2011, **115**, 15280–15288.
24 E. A. Turner, C. C. Pye and R. D. Singer, *J. Phys. Chem. A*, 2003, **107**, 2277–2288.
25 O. Russina, A. Triolo, L. Gontrani and R. Caminiti, *J. Phys. Chem. Lett.*, 2012, **3**, 27–33.
26 H. V. R. Annapureddy, H. K. Kashyap, P. M. De Biase and C. J. Margulis, *J. Phys. Chem. B*, 2010, **114**, 16838–16846.
27 C. Hardacre, J. D. Holbrey, C. L. Mullan, T. G. A. Youngs and D. T. Bowron, *J. Chem. Phys.*, 2010, **133**, 074510.
28 J. N. A. Canongia Lopes and A. A. H. Pádua, *J. Phys. Chem. B*, 2006, **110**, 3330–3335.
29 P. D'Angelo, V. Migliorati, G. Mancini and G. Chillemi, *J. Phys. Chem. A*, 2008, **112**, 11833–11841.
30 G. Mancini, N. Sanna, V. Barone, V. Migliorati, P. D'Angelo and G. Chillemi, *J. Phys. Chem. B*, 2008, **112**, 4694–4702.
31 V. Migliorati and P. D'Angelo, *RSC Adv.*, 2013, **3**, 21118–21126.
32 V. Migliorati, F. Sessa, G. Aquilanti and P. D'Angelo, *J. Chem. Phys.*,

2014, **141**, 044509.
33 V. Migliorati, G. Mancini, S. Tatoli, A. Zitolo, A. Filipponi, S. De Panfilis, A. Di Cicco and P. D'Angelo, *Inorg. Chem.*, 2013, **52**, 1141–1150.
34 P. D'Angelo, V. Migliorati, G. Mancini, V. Barone and G. Chillemi, *J. Chem. Phys.*, 2008, **128**, 084502.
35 V. Migliorati, A. Zitolo and P. D'Angelo, *J. Phys. Chem. B*, 2013, **117**, 12505–12515.
36 V. Migliorati, A. Zitolo, G. Chillemi and P. D'Angelo, *ChemPlusChem*, 2012, **77**, 234–239.
37 V. Migliorati, G. Chillemi and P. D'Angelo, *Inorg. Chem.*, 2011, **50**, 8509–8515.
38 W. Smith and T. Forester, *J. Mol. Graphics*, 1996, **14**, 136–141.
39 J. N. Canongia Lopes, J. Deschamps and A. A. H. Pádua, *J. Phys. Chem. B*, 2004, **108**, 2038–2047.
40 J. N. Canongia Lopes and A. A. H. Pádua, *J. Phys. Chem. B*, 2006, **110**, 19586–19592.
41 W. L. Jorgensen, J. P. Ulmschneider and J. Tirado-Rives, *J. Phys. Chem. B*, 2004, **108**, 16264–16270.
42 S. Nosé, *J. Chem. Phys.*, 1984, **81**, 511–519.
43 D. J. Evans and B. L. Holian, *J. Chem. Phys.*, 1985, **83**, 4069–4074.
44 U. Essmann, L. Perera, M. L. Berkowitz, T. Darden, H. Lee and L. G. Pedersen, *J. Chem. Phys.*, 1995, **103**, 8577–8593.
45 J.-P. Ryckaert, G. Ciccotti and H. J. Berendsen, *J. Comput. Phys.*, 1977, **23**, 327–341.
46 M. Brehm and B. Kirchner, *J. Chem. Inf. Model.*, 2011, **51**, 2007–2023.
47 C. J. Pings and J. J. Waser, *J. Chem. Phys.*, 1968, **48**, 3016.
48 V. Migliorati, P. Ballirano, L. Gontrani, O. Russina and R. Caminiti, *J. Phys. Chem. B*, 2011, **115**, 11805–11815.
49 V. Migliorati, P. Ballirano, L. Gontrani, S. Materazzi, F. Ceccacci and R. Caminiti, *J. Phys. Chem. B*, 2013, **117**, 7806–7818.
50 A. Di Cicco, G. Aquilanti, M. Minicucci, E. Principi, N. Novello, A. Cognigni and L. Olivi, *J. Phys.: Conf. Ser.*, 2009, **190**, 012043.
51 A. Filipponi and A. Di Cicco, *Phys. Rev. B*, 1995, **52**, 15135–15149.
52 A. Filipponi, A. Di Cicco and C. R. Natoli, *Phys. Rev. B*, 1995, **52**, 15122–15134.
53 A. Triolo, O. Russina, B. Fazio, R. Triolo and E. D. Cola, *Chem. Phys. Lett.*, 2008, **457**, 362 – 365.
54 C. Chiappe, *Monatsh. Chem.*, 2007, **138**, 1035–1043.
55 Y. Umebayashi, H. Hamano, S. Tsuzuki, J. N. Canongia Lopes, A. A. H. Pádua, Y. Kameda, S. Kohara, T. Yamaguchi, K. Fujii and S.-i. Ishiguro, *J. Phys. Chem. B*, 2010, **114**, 11715–11724.
56 M. Chen, R. Pendrill, G. Widmalm, J. W. Brady and J. Wohlert, *J. Chem. Theory Comput.*, 2014, **10**, 4465–4479.
57 G. Raabe and J. Khler, *J. Chem. Phys.*, 2008, **128**, 154509.
58 M. G. Del Pópolo, R. M. Lynden-Bell and J. Kohanoff, *J. Phys. Chem. B*, 2005, **109**, 5895–5902.
59 Z. Liu, T. Chen, A. Bell and B. Smit, *J. Phys. Chem. B*, 2010, **114**, 4572–4582.
60 H. Hamaguchi and R. Ozawa, *Adv. Chem. Phys.*, 2005, **131**, 85–104.